Optimal power dispatch considering load and renewable generation uncertainties in an AC–DC hybrid microgrid

Article *in* IET Generation Transmission & Distribution · January 2019

DOI: 10.1049/iet-gtd.2018.6502

2 authors, including:

Avirup Maulik
Pandit Deen Dayal Petroleum University
14 PUBLICATIONS **72** CITATIONS

SEE PROFILE

EMISSION LOAD DISPATCH;

IET Research Journals

Submission Template for IET Research Journal Papers

IET Journals
The Institution of Engineering and Technology

Optimal power dispatch considering load and renewable generation uncertainties in an AC-DC hybrid microgrid

ISSN 1751-8644
doi: 0000000000
www.ietdl.org

Avirup Maulik[1*], *Debapriya Das*[2]

[1] *Electrical Engineering Department, Indian Institute of Technology Kharagpur, Kharagpur, India*
[2] *Electrical Engineering Department, Indian Institute of Technology Kharagpur, Kharagpur, India*
[*] *E-mail: avirupmaulik@gmail.com*

Abstract:
An AC-DC hybrid microgrid is gradually becoming popular. For economic viability and environmental sustainability, an AC-DC microgrid should be operated optimally. This paper introduces an optimal power dispatch strategy for simultaneous reduction of cost and emission from generation activities in an AC-DC hybrid microgrid under load and generation uncertainties. The operational attributes of an AC-DC hybrid microgrid, and load and renewable generation uncertainties are incorporated in the optimal scheduling problem by using a customized power-flow technique, and by modeling uncertainties by Hong's two-point estimate method respectively. The economic and environmental objectives are modeled in the fuzzy domain by fuzzy membership functions. A combination of particle swarm optimization and fuzzy max-min technique is then employed for obtaining the optimal solution. The static active power droop constants of the dispatchable units are the control variables. Simulation results on a 6-bus AC-DC hybrid microgrid system demonstrate that optimal scheduling results in 4.26% reduction of operating cost and 13.91% reduction of emission in comparison to capacity based droop settings. Further, a comparison between the proposed method and the elitist multi-objective GA indicates that the optimized solution lies on the Pareto-front, thereby validating the proposed technique.

Nomenclature

Variables

$\mathbf{Z}$	Vector of the stochastic output variable
p_l	l^{th} random input variable
m	Total number of random input variables
F	Equation set relating the input & output variables
$p_{l,k}, w_{l,k}, \xi_{l,k}$	Location, weight, & standard location of l^{th} input variable in the k^{th} concentration
$\lambda_{l,3}, M_3(p_l)$	coefficient of skewness & third moment of p_l respectively
f_{p_l}	Probability density function of p_l
$E(\mathbf{Z}), E(\mathbf{Z}^j)$	Expected value & j^{th} moment of the output variable $\mathbf{Z}$ respectively
V_i, ω	Voltage of the i^{th} bus & the system frequency
δ_i	Voltage angle of the i^{th} bus in the ACMG
V_{0i}, ω_{0i}	Reference voltage & frequency of the dispatchable DG unit at the i^{th} bus
m_{Pi}, n_{Qi}	Static active & reactive power droop constants of the dispatchable DG unit at the i^{th} bus
PG_i, QG_i	Active and reactive power output of the dispatchable DG unit at the i^{th} bus
PL_i, QL_i	Active and reactive load at the at the i^{th} bus
$PGND_i$	Active power generated by the non-dispatchable DG unit at the i^{th} bus
$QGND_i$	Reactive power generated by the non-dispatchable DG unit at the i^{th} bus
$\hat{\omega}, \hat{V}_{dc}$	Normalized frequency and DC voltage
V_{dc}, V_{int}	Voltages at the DC terminal & interlinking bus
Δe	Error signal
P_{ic}, Q_{ic}	Active and reactive power of interlinking converter
$\lvert Y_{ik}(\omega)\rvert$	Magnitude of the ik^{th} element of the Y-bus matrix
$\theta_{ik}(\omega)$	Phase of the ik^{th} element of the Y-bus matrix
G_{ik}	ik^{th} element of bus conductance matrix
$f_{sol}(.)$	Probability density function (PDF) of the solar irradiance
S	Solar irradiance (kW/m^2)
P_S	Output active power of PV module
$f_{wind}(.)$	PDF of the wind speed
v	wind speed in m/s
P_W	Active power output of wind turbine
PL	Random variable representing actual load L
$f_{load}(.)$	PDF of PL
OF_1, OF_2	Expected operating cost & emission respectively
f_{fueli}	fuel consumption of the i^{th} dispatchable DG unit
$F_l(.)$	Set of power flow equations under loading condition l
g_l	Set of power flow state variables
τ_l	Set of droop parameters of the dispatchable DG unit
$\{c, m\}$	Allowable range of state variables
I_b	Current in the b^{th} line
μ_C, μ_E	Membership function value for cost & emission minimization respectively
OF_1^{min}, OF_1^{max}	Minimum & maximum values of OF_1 respectively
OF_2^{min}, OF_2^{max}	Minimum & maximum values of OF_2 respectively
$\vec{Vel}_{it}, \vec{X}_{it}$	Velocity vector & Position vector in PSO
$\vec{P}_{it}, \vec{PG}$	Local & global best in PSO

Parameters

μ_{pl}, σ_{pl}	Mean & standard deviation respectively

		of the l^{th} random input variable
γ_p, γ_q		Static active & reactive power droop constants of the interlinking converter
Solar cells		
$\Gamma()$		gamma function
μ_s, σ_s		Mean & standard deviation respectively of the solar irradiance
α, β		Shape parameters of the beta distribution
T_C, T_A, N_{OT}		Cell, ambient, & nominal operating temperature respectively ($^\circ C$)
K_v		Voltage temperature coefficient ($V/^\circ C$)
K_i		current temperature coefficient ($A/^\circ C$)
V_{OC}		Open circuit voltage (in V)
V_{MPP}		Voltage at maximum power point (in V)
I_{SC}		Short circuit current (in A)
I_{MPP}		Current at maximum power point (in A)
FF		Fill factor
Wind turbine		
k		Shape index of Weibull distribution
c		Scale index of Weibull distribution
v_{ci}		Cut in speed in m/s
v_r		Rated speed in m/s
v_{furl}		Furling speed in m/s
P_{Wr}		Rated power of the wind turbine
Load		
N		Normal distribution
μ_L, σ_L		Mean & standard deviation of load
Dispatchable unit	:	**Parameters for the i^{th}unit**
K_{fueli}, K_{mi}		Fuel Price and maintenance cost
η_{iP}		Power efficiciency
K_{ei}		Carbon foot print
f_{fueli}		Fuel consumption
PG_i^{min}, PG_i^{max}		Minimum & maximum active power limits
QG_i^{min}, QG_i^{max}		Minimum & maximum reactive power limits
UR_i and DR_i		Ramp up and ramp down limits
Others		
I_b^{rated}		Current rating of the b^{th} line
$G_{droopac}$		Set of all droop controlled units in the AC sub-system
$G_{droopdc}$		Set of all droop controlled units in the DC sub-system
$\omega_{max}, \omega_{min}$		Maximum & Minimum allowable frequency of the AC sub-system
V_{dcmax}, V_{dcmin}		Maximum & Minimum allowable voltage of the DC sub-system
n_{ac}		Number of buses in the AC sub-system
Ω_{ac}		Set of all AC sub-system buses
$\Omega_{acintlink}$		Set of interlinking terminal buses in the AC sub-system
$\perp$		Complement
n_{dc}		Number of buses in the DC sub-system
Ω_{dc}		Set of all buses in the DC sub-system
$\Omega_{dcintlink}$		Set of interlinking terminal buses in the DC sub-system
n_G^{ac}		Numbers of dispatchable units in the AC sub-system
n_G^{dc}		Numbers of dispatchable units in the DC sub-system
Ω_{droop}^{ac}		Set of droop buses in the AC sub-system
Ω_{droop}^{dc}		Set of droop buses in the DC sub-system
Nl		Set of all lines
NP, wt_{pso}, it		Population, weight, & iteration number of PSO respectively

1 Introduction

1.1 Motivation

For serving an area comprising both DC and AC sources and loads, researchers have proposed the concept of AC-DC hybrid microgrid (ADHMG) [1–3]. An ADHMG comprises AC microgrids (ACMG) and DC microgrids (DCMG) dovetailed through bi-directional interlinking converters [1–3, 7]. An ADHMG has the following operational features:

1. Autonomous load sharing among dispatchable DG units takes place as per primary droop control strategy. Active power and reactive power are shared as per P-f and Q-V characteristic respectively in an AC sub-grid; active power is shared as per I-V or P-V characteristic in a DC sub-grid [4–7].
2. Power transfer between AC and DC sub-grids takes place autonomously via inter-linking converters depending on relative loadings of the sub-grids. Several suitable operation and control strategies for stable operation of an ADHMG have been reported in literature. Autonomous power exchange between AC and DC sub-grids takes place (via interlinking converter) such that neither the ACMG nor the DCMG are overloaded or under-loaded with respect to each other [1–3, 7].

Due to the above operational features, traditional power flow algorithms are not applicable to an ADHMG. Therefore, power flow algorithms embodying the above special operational features were developed for accurate steady state analysis of ADHMG [8–13]. However, apart from stable and robust control operation, it is also obligatory that the ADHMG be operated optimally for financial viability and environmental sustainability.

1.2 Literature survey

Recently, some researchers have focused on determining the optimal dispatch strategy of an ADHMG. A mixed integer linear model aimed at minimizing total operating cost (over a 24-hour period) in an ADHMG was presented in [14]. A suitable supervisory control strategy for power management in an ADHMG was suggested in [15]. Goals in [15] were to use maximum renewable power, sustain state of charge (SOC) of battery banks, and suitably manage power transfer between AC and DC sub-grids. A robust control strategy was proposed in [16]. Objectives of the control strategy in [16] were maximum usage of renewable power, minimum usage of fuel-based generation units, improving battery lifetime, and curbing the usage of the interlinking converter. Li et al. [17] introduced a technique for bettering the economic benefit of an ADHMG under spot price mechanism regime. A double-uncertainty optimization theory was proposed by Peng et al. [18] to handle renewable energy uncertainty while minimizing operating cost in an ADHMG. Analytical target cascading (ATC) based decentralized optimal operation strategy was suggested by Qi et al. [19] for minimizing the operation cost in an ADHMG. Hussain et al. [20] presented a robust optimization method for minimizing the operation cost of an ADHMG under market price and renewable generation uncertainties. Therefore, only a few papers have dealt with optimal operation of ADHMG, and a lot of research work is required in this area.

1.3 Contributions of the paper

In this paper, we have concentrated on expanding the aforementioned threads of work [14–20] by overcoming their shortcomings. The shortcomings of the papers reported so far and the contributions of this paper in connection to the same are detailed below:

- *Incorporation of the special operating attributes of an AC-DC hybrid microgrid*: Most of the papers dealing with optimal ADHMG operation have neglected the special operational features of ADHMG (primary level droop control and operation of the inter-linking converter) while formulating the optimization problem

IET Research Journals, pp. 1–13

[14–20]. As a consequence, an accurate picture of the steady state condition of the system cannot be obtained from the above work. In this paper, we have eliminated the afore-mentioned shortcoming by incorporating the primary droop controls of ACMG, DCMG and interlinking converter in the ADHMG model. In this paper, a power flow algorithm tailor-made for ADHMG [8–13] is used as a subroutine of the bi-objective optimal scheduling problem for accurately determining the steady state operating conditions.

- *Considering environmental objective along with economic objective*: Environmental sustainability, economic viability, energy security, air pollution and climate change are driving forces of present-day world energy policy [21–23]. Therefore, contemporary energy policy emphasizes on an environment-friendly, sustainable, low-cost and accessible energy system [21–23]. In this context, it is crucial to generate power not only at reduced cost, but also with reduced emission. However, to the best of author's knowledge, the issue of reduced emission from generation activities in an ADHMG has not been addressed as far [14–20]. In this paper, we have suggested an uncomplicated optimization model for simultaneous reduction of operating cost and emission. Out of many available methods for solving multi-objective optimization, fuzzy max-min approach is used in this paper due to its effectiveness and simplicity [28]. The optimization problem is solved using particle swarm optimization (PSO), which has exhibited good performance in solving various engineering problems [29–32]. The proposed optimization algorithm can be implemented in the energy management system (EMS) of the ADHMG. EMS collects necessary information like load and renewable generation forecasts along with associated uncertainties, dispatchable DG unit cost and emission characteristics, network parameters and configuration through low-bandwidth communication channels for carrying out the optimization. Optimal droop parameters (obtained as output of the optimization program) are communicated to individual local controllers for implementation at primary level through low-bandwidth communication channels. Communication channels are used only for to and fro communication between local controllers and the EMS. At other times, communication channels are not required. In case of failures of communication links, the system continues to operate with last calculated droop values. Thus communication link unavailability does not jeopardize or hamper the system operation, there might only be a temporary deviation from optimal operation.
- *Considering load and renewable generation uncertainties*: Load demands and renewable generations are uncertain in nature. Soundness of deterministic approaches depends on accuracy of input data. It is therefore essential to model uncertainties present in a system to reduce the risk of dispatch strategy of microgrid [23, 24, 27]. But many papers ([14–17, 19]) on optimal operation of ADHMG have neglected load and renewable generation uncertainties. Only in [18], renewable generation uncertainty was considered, and in [20], market price and renewable generation uncertainties were considered. In this paper, we have modeled and incorporated load and renewable generation uncertainties in the optimal scheduling problem. Out of many available approaches for modeling uncertainties (like probabilistic approach, possibilistic approach, hybrid probabilistic-possibilistic technique, information gap decision theory (IGDT), robust optimization and interval analysis [23, 25, 26]), probabilistic approach is most commonly used for modeling load and renewable generation uncertainties [23, 24]. Probabilistic techniques can broadly be grouped into three heads: Monte carlo simulation (MCS), Analytical approaches and approximate methods [23, 25, 26]. MCS technique is accurate, but it involves large computational burden [23, 25, 26]. Analytical techniques (convolution method, cumulants technique, Taylor series expansion) demand lesser computational effort in comparison to MCS approach, but they require complicated mathematics [23, 25, 26]. Approximate techniques provide a fare trade-off between accuracy and computational load. Two widely used approximate techniques are scenario-based approach and point estimate method (PEM)[23, 25, 26]. Scenario-based approach is uncomplicated, but its accuracy depends on number of states considered. Also, only mean values are obtainable from scenario based approach. PEM determines statistical moments of a random quantity. PEM has been widely employed in various power system applications [23]. In this paper, we have used Hong's $2m$ point estimate method for modeling and incorporating uncertainties associated with load and renewable generation.
- *Performance evaluation*: The proposed optimal scheduling strategy is tested on a 6 bus test AC-DC hybrid microgrid system. Different scenarios with different objectives are simulated. Simulation results demonstrate that different objectives can be met successfully by optimally setting the static active power droop constants of the dispatchable units in the ADHMG. If the lone objective is to minimize the cost, then a maximum cost saving of 35.87% can be achieved in comparison to the capacity based droop setting for the given system. Similarly, with the lone objective of emission reduction, the emission may be reduced by about 73.10% by optimally setting the droop values. However, if cost and emission are to be simultaneously reduced, then a cost saving to the tune of 4.26% and a reduction in emission by about 13.91% can be achieved for the given system. A comparison with the cost-prioritized droop and the emission-prioritized droop scheme illustrates that the proposed method yields better results. A comparison of results of the proposed bi-objective optimal scheduling problem with controlled elitist multi-objective genetic algorithm (GA) demonstrates that the proposed optimization method yields solution on the pareto front. Since, controlled elitist multi-objective GA [67] is a well established method of solving multi-objective optimization problems, a close proximity of results validates the proposed method. However, the advantage of the proposed method is the simplicity in coding and implementation.

Fig.1 gives a big picture schematic overview of the paper.

1.4 Organization of the paper

The organization of the remainder of this paper is as follows. In section 2, Hong's two point estimate method is discussed. In section 3, we have modeled the various components of the ADHMG. In section 4, the optimization problem is formulated by considering the objective functions and various system constraints. Section 5 deals with the solution strategy of the bi-objective optimal scheduling problem in the fuzzy domain. In section 6, simulation results are provided, followed by conclusions in section 7.

2 Hong's Point estimate method (PEM)

Rosenblueth [34] had proposed $2m$ point estimate method (PEM) in 1975. However, the method was inefficient [24]. A more efficient version of PEM was proposed by Harr in 1989 [35]. However, Harr's version could handle only symmetric variables [23, 24]. Hong suggested an efficient PEM in 1998 [36]. Hong's method is capable of dealing with both symmetric and asymmetric variables. In this paper, we have employed Hong's PEM to model load and renewable generation uncertainties.

If $\mathbf{Z}$ is a vector of stochastic output variable, and p_l is the l^{th} random input variable, then [23, 24]:

$$\mathbf{Z}(l,k) = F(p_1, p_2, \cdots, p_l, \cdots, p_m) \tag{1}$$

where m is the total number of uncertain/random input variables, F is the set of equations that describe the relation between input and output, k denotes the k^{th} concentration. PEM gathers statistical information from first central moments of stochastic input variables, and use the information to determine K points for each stochastic input variable. The k^{th} concentration ($p_{l,k}$, $w_{l,k}$) comprises a location ($p_{l,k}$) and its corresponding weight ($w_{l,k}$) [23, 24, 37–40]. While the location denotes the k^{th} value of the input random variable p_l at which F is evaluated, the weight $w_{l,k}$ signifies the relative importance of this evaluation [23, 24, 37–40]. The function (F) is computed K times for each random variable p_l. While evaluating the random variable p_l, remaining $m-1$ random variables are set to their mean values ($\mu_{pi}, i = 1, 2, \cdots, m; i \neq l$). If $\mathbf{Z}(l,k)$ be the

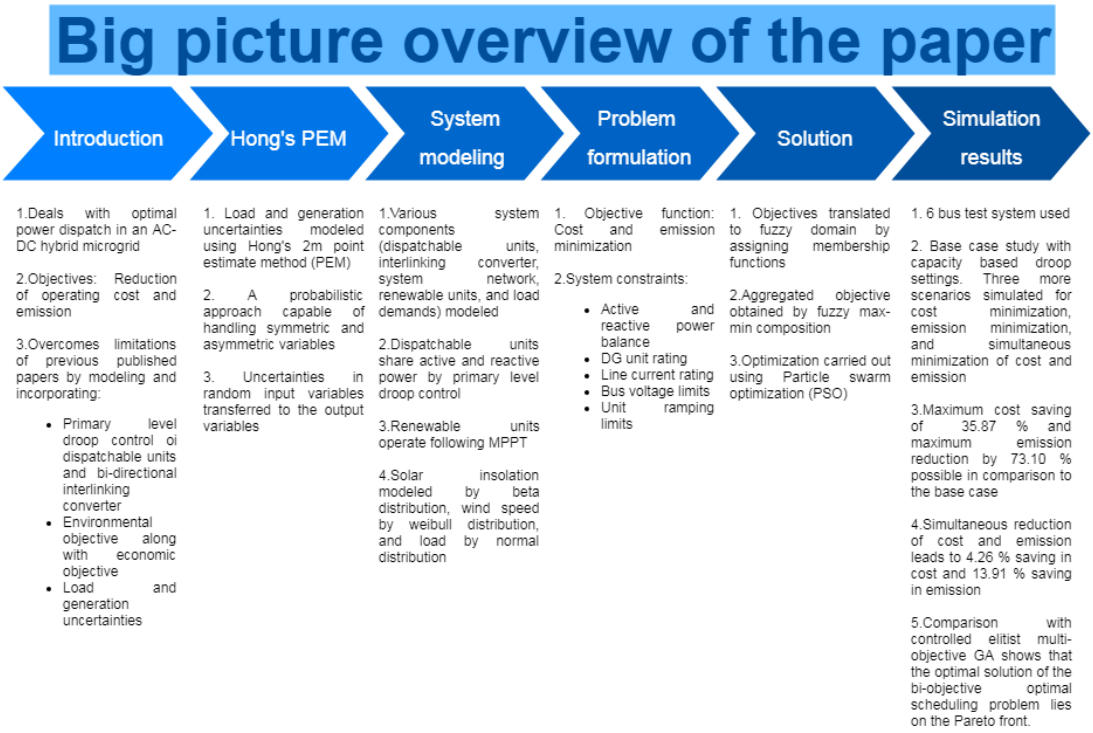

Fig. 1: Big picture schematic overview of the paper

set of stochastic output variables for the k^{th} concentration of the l^{th} random input variable, we may write the following:

$$\mathbf{Z}(l,k) = F(\mu_{p1}, \mu_{p2}, \cdots, p_{l,k}, \cdots, \mu_{pm}) \tag{2}$$

For $2m$ PEM method, there are $2m$ evaluations. Location $p_{l,k}$ is given by the following [23]:

$$p_{l,k} = \mu_{pl} + \xi_{l,k}\sigma_{pl} \tag{3}$$

where μ_{pl}, σ_{pl}, ξ_{lk} are respectively the mean, standard deviation and standard location of the l^{th} random input variable. The standard location for a $2m$ scheme is given by the following [23]:

$$\xi_{l,k} = \frac{\lambda_{l,3}}{2} + (-1)^{3-k}\sqrt{m + (\frac{\lambda_{l,3}}{2})^2} \quad for \quad k = 1, 2. \tag{4}$$

The weight $w_{l,k}$ can take values between 0 and 1 and sum of weights add upto 1. In Hong's $2m$ PEM, the weights are given as follows [23]:

$$w_{l,k} = \frac{1}{m}(-1)^k \frac{\xi_{l,3-k}}{\zeta_l} \quad for \quad k = 1, 2 \tag{5}$$

$$\zeta_l = 2\sqrt{m + (\frac{\lambda_{l,3}}{2})^2} \tag{6}$$

The coefficient of skewness $\lambda_{l,3}$ is calculated as below [23]:

$$\lambda_{l,3} = \frac{M_3(pl)}{(\sigma_{pl})^3} \tag{7}$$

$M_3(pl)$ is the third moment of pl given as follows [23]:

$$M_3(pl) = \int_{-\infty}^{\infty} (p_l - \mu_{pl})^3 f_{pl} \mathrm{d}pl \tag{8}$$

Uncertainties involved with load demand and renewable generation are modeled using Hong's $2m$ PEM as described above. The uncertain input variables are described by their probability density functions. It has been observed that load demand error closely follows normal distribution [23, 24]. Similarly, solar insolation follows beta distribution [23], and wind velocity follows Weibull distribution [24]. For every uncertain input variable (wind power, solar power, load demand), the concentrations are calculated. These concentrations are used to carry out a deterministic analysis for each point in the concentration. The process is repeated for all concentrations for all input random variables. The objective functions and other output variables are expressed in the form of (2). Therefore, at any iteration step of the PSO program, for each member of the population, we carry out $2m$ evaluations. Raw moments of output variables are determined as below:

$$\mathbf{E}(\mathbf{Z}) = \sum_{k=1}^{2}\sum_{l=1}^{m} w_{l,k}\mathbf{Z}(l,k) \tag{9}$$

$$\mathbf{E}(\mathbf{Z^j}) = \sum_{k=1}^{2}\sum_{l=1}^{m} w_{l,k}(\mathbf{Z}(l,k))^j \tag{10}$$

where $E(Z^j)$ is the j^{th} moment of the output variable Z

3 Modeling of system components

3.1 Dispatchable DG unit model in ACMG

In an ACMG, dispatchable DG units can either operate as droop controlled units or as constant PQ unit. For the i^{th} droop controlled unit in the ACMG, following relations apply [10]:

$$\begin{aligned} \omega &= \omega_{0i} - m_{Pi} \times PG_i \quad \forall i \in G_{droopac} \\ |V_i| &= |V_{0i}| - n_{Qi} \times QG_i \quad \forall i \in G_{droopac} \end{aligned} \tag{11}$$

where ω is the system frequency, ω_{0i} and $|V_{0i}|$ are respectively the frequency and voltage references for the DG unit, $|V_i|$ is the voltage magnitude of the bus to which the DG unit is connected, m_{Pi} and n_{Qi} are the static active and reactive power droop constants respectively, PG_i and QG_i are the active and reactive power outputs respectively, $G_{droopac}$ is the set of all droop controlled units in the ACMG. Dispatchable DG units working in PQ mode inject constant active and reactive power to the network. They are modeled as constant power sources or negative constant loads in the power flow model.

3.2 Dispatchable DG unit model in DCMG

A dispatchable DG unit working in droop controlled mode in the DCMG follows the following equation [10]:

$$V_i = V_{0i} - m_{Pi} \times PG_i \quad \forall i \in G_{droopdc} \tag{12}$$

where V_i is the voltage of the bus to which the DG unit is connected, V_{0i} is the voltage reference to the DG unit, m_{Pi} is the static active power droop constant, PG_i is the power output of the DG unit, $G_{droopdc}$ is the set of all droop controlled units in the DCMG. Dispatchable units operating in constant P mode are modeled as constant power sources or negative loads in the power flow formulation.

3.3 Interlinking converter

Interlinking converter acts like an energy buffer and autonomously regulates power exchange between AC and DC sub-grid so that neither the AC nor the DC sub-grid gets over-loaded or under-loaded. Frequency of the AC sub-grid and voltage at the DC terminal are measured and normalized in a range between [-1 1] as given below [9, 10]:

$$\begin{aligned} \hat{\omega} &= \frac{\omega - \frac{(\omega_{max}+\omega_{min})}{2}}{\frac{(\omega_{max}-\omega_{min})}{2}} \\ \hat{V_{dc}} &= \frac{V_{dc} - \frac{(V_{dcmax}+V_{dcmin})}{2}}{\frac{(V_{dcmax}-V_{dcmin})}{2}} \end{aligned} \tag{13}$$

The normalized frequency and DC voltage are used to calculate an error signal (Δe), which in turn is used to autonomously determine the direction and magnitude of power exchange between AC and DC sub-grids [9, 10]:

$$\begin{aligned} \Delta e &= \hat{\omega} - \hat{V_{dc}} \\ P_{ic} &= -\frac{\Delta e}{\gamma_p} \end{aligned} \tag{14}$$

where P_{ic} is the power handled by interlinking converter, γ_p is the active power static droop gain of the interlinking converter. If $\Delta e > 0$, AC sub-grid is under-loaded in comparison to DC sub-grid. Therefore, active power is transferred from AC to DC side ($P_{ic} < 0$). If $\Delta e < 0$, DC sub-grid is under-loaded in comparison to AC sub-grid. Therefore, active power is transferred from DC to AC side ($P_{ic} > 0$). The interlinking converter also supplies reactive power to the AC sub-grid depending on the voltage difference between the nominal and actual bus voltage at the interlinking terminal [9]:

$$Q_{ic} = \frac{|V_{nom}| - |V_{int}|}{\gamma_q} \tag{15}$$

where $|V_{nom}|$ and $|V_{int}|$ are respectively the nominal and actual voltage values at the interlinking bus in the AC sub-grid, Q_{ic} is the reactive power supplied by the interlinking converter, and γ_q is the static reactive power drop gain of the interlinking converter.

3.4 Network modeling and power flow equations

The network is modeled by power flow equations as given below:

3.4.1 AC microgrid: : Power flow equations are given below [9, 10]:

$$\begin{aligned} fp_{ac,i} &= |V_i| \sum_{k=1}^{n_{ac}} |V_k||Y_{ik}(\omega)|cos(\delta_i - \delta_k - \theta_{ik}(\omega)) \\ &\quad + \beta_i P_{ic,i} \quad \forall i \in \Omega_{ac} \\ fq_{ac,i} &= |V_i| \sum_{k=1}^{n_{ac}} |V_k||Y_{ik}(\omega)|sin(\delta_i - \delta_k - \theta_{ik}(\omega)) \\ &\quad + \beta_i Q_{ic,i} \quad \forall i \in \Omega_{ac} \\ \beta_i &= 1 \quad \forall i \in \Omega_{acintlink} \\ &= 0 \quad otherwise \end{aligned} \tag{16}$$

where $|V_i|$ and δ_i are voltage magnitude and angle of the i^{th} bus in the ACMG, $|Y_{ik}(\omega)|$ and $\theta_{ik}(\omega)$ are magnitude and phase of the ik^{th} element of the Y-bus matrix, n_{ac} is the number of buses in the ACMG, Ω_{ac} is the set of all ACMG buses, $\Omega_{acintlink}$ is the set of interlinking terminal buses in the ACMG. For the i^{th} bus, we have:

$$\begin{aligned} fp_{ac,i} &= PG_i + PGND_i - PL_i \\ fq_{ac,i} &= QG_i + QGND_i - QL_i \end{aligned} \tag{17}$$

where PG_i and QG_i are respectively the active and reactive power output of the dispatchable DG unit connected to the i^{th} bus, $PGND_i$ and $QGND_i$ are respectively the active and reactive power injections from renewable generation source, PL_i and QL_i are respectively the active and reactive loads at the i^{th} bus.

The fact that a droop controlled unit may switch over to constant PQ mode when its rating is exceeded can be compactly represented by using the concept and notation of non-linear complementary constraint [41] as given below:

$$\begin{aligned} 0 \leq PG_i^{max} - PG_i \perp \frac{\omega_{0i} - \omega}{m_{Pi}} - PG_i \geq 0 \\ 0 \leq QG_i^{max} - QG_i \perp \frac{|V_{0i}| - |V_i|}{n_{Qi}} - QG_i \geq 0 \end{aligned} \tag{18}$$

where PG_i^{max} and QG_i^{max} respectively denote rated active and reactive power of the dispatchable DG unit connected to bus i, $\perp$ denotes complement.

3.4.2 DCMG: In a DCMG, the power flow equations are as follows [9, 10]:

$$\begin{aligned} fp_{dc,i} &= V_i \sum_{k=1}^{n_{dc}} V_k G_{ik} - \beta_i P_{ic,i} \quad \forall i \in \Omega_{dc} \\ \beta_i &= 1 \quad \forall i \in \Omega_{dcintlink}; \quad \beta_i = 0 \quad otherwise \end{aligned} \tag{19}$$

where V_i denotes bus voltage, G_{ik} is the ik^{th} element of bus conductance matrix, n_{dc} denotes the number of buses in the DCMG,

Ω_{dc} stands for the DCMG bus sets, $\Omega_{dcintlink}$ denotes the set of interlinking buses in the DCMG. $f_{pdc,i}$ is also given by(17). In DCMG also, we can use non-linear complementary constraints to write:

$$0 \leq PG_i^{max} - PG_i \perp \frac{V_{0i} - V_i}{m_{Pi}} - PG_i \geq 0 \tag{20}$$

Power flow algorithm for ADHMG [8–13] is used for solving the set of non-linear equations.

3.5 Modeling of renewable power sources

Renewable power DG units (solar and wind) do not have fuel cost. They operate following maximum power point tracking (MPPT) algorithm for harnessing maximum available power. In power flow formulations, they are considered as negative loads. Probabilistic modeling of solar photovoltaic (SPV) cells and wind turbine (WT) generators are given below:

3.5.1 Solar photovoltaic cells: The probability density function (PDF) of solar irradiance ($f_{sol}(S)$) is modeled by beta distribution [23, 42, 43] as given below:

$$f_{sol}(S) = \frac{\Gamma(\alpha+\beta)}{\Gamma(\alpha)\Gamma(\beta)}(S)^{\alpha-1}(1-S)^{\beta-1} \tag{21}$$

where S denotes the solar irradiance (kW/m^2, Γ denotes gamma function. Shape parameters (α, β) of the beta distribution are related to mean (μ_s) and standard deviations (σ_s) by following [23, 43]:

$$\beta = (1-\mu_s)(\frac{\mu_s(1+\mu_s)}{(\sigma_s)^2} - 1); \quad \alpha = \frac{\mu_s\beta}{1-\mu_s} \tag{22}$$

The output power of a solar photovoltaic cell has a non-linear relationship with the solar insolation. In [42], the authors used the non-linear equivalent circuit of a solar module to derive a mathematical model for determining the output power of a PV module from the solar insolation data. The model has been used widely for stochastic studies of solar photovoltaic power [43–48]. We have used the same model for stochastic modeling of the power output from the PV module.Output power of PV module (P_S) is computed using the following [43]:

$$\begin{aligned} &T_c = T_A + S(\frac{N_{OT}-20}{0.80}); I = S[I_{SC} + K_i(T_c - 25)] \\ &V = V_{OC} - K_v T_C; FF = \frac{V_{MPP}I_{MPP}}{V_{OC}I_{SC}} \\ &P_S = N \times FF \times V \times I \end{aligned} \tag{23}$$

where T_C, T_A, and N_{OT} are the cell, ambient, and nominal operating temperature respectively ($^\circ C$), K_v and K_i denote voltage temperature coefficient ($V/^\circ C$) and current temperature coefficient ($A/^\circ C$)respectively, V_{OC} and V_{MPP} denote open circuit voltage and voltage at maximum power point respectively (in V), I_{SC} and I_{MPP} denote the short circuit current and current at maximum power point respectively (in A), FF is the fill factor.

3.5.2 Wind turbine: Wind speed PDF ($f_{wind}(v)$) can be modeled by Weibull distribution given as follows [41, 43]:

$$f_{wind}(v) = \frac{k}{c}(\frac{v}{c})^{k-1}\exp[-(\frac{v}{c})^k] \tag{24}$$

where v is the wind speed in m/s, k is the shape index, c is the scale index.

Power of wind turbine (P_W) is calculated as follows [41, 43]:

$$\begin{aligned} P_W &= 0 \quad for \quad 0 \leq v \leq v_{ci} \quad or \quad v \geq v_{furl} \\ &= P_{Wr}\frac{v - v_{ci}}{v_r - v_{ci}} \quad if \quad v_{ci} \leq v \leq v_r \\ &= P_{Wr} \quad otherwise \end{aligned} \tag{25}$$

where v, v_{ci}, v_r, v_{furl} denote the wind speed, cut in speed rated speed, and furling speed respectively in m/s, P_{Wr} is the rated power of the wind turbine.

In reality, there is a slight non-linearity in the relationship between the output power of a wind energy conversion system and the wind velocity between the cut-in speed and the rated speed. Sometimes, the datasheet provided by the manufacturer contains the non-linear relationship. In such cases, (25) may be suitably modified. However, in many instances, the slight non-linearity is neglected, and the datasheet provides an approximately linear relationship between the output power and the wind speed [50]. The error introduced by this approximation is small, and hence, in most of the papers dealing with stochastic modeling of wind power, the authors have neglected the slight non-linearity [37, 41, 43, 49–53]. In this paper, in line with the previous threads of work on stochastic modeling of wind power [37, 41, 43, 49–53], we have neglected the slight non-linearity since it does not introduce any significant error.

3.6 Modeling of load uncertainty

Load uncertainty is modeled using normal distribution as given below [54]:

$$PL \sim N(\mu_L, \sigma_L); \quad f_{load}(L) = \frac{1}{\sigma_L\sqrt{2\pi}}e^{\frac{-(L-\mu_L)^2}{2\sigma_L^2}} \tag{26}$$

where N denotes normal distribution, PL is a random variable representing the actual load, μ_L and σ_L represent the mean and standard deviation of PL respectively, $f_{load}(L)$ is the probability density function of PL.

4 Problem formulation

Two objectives are minimization of operating cost and emission.

4.1 Objective function

The combined objective can be expressed as follows:

$$\begin{aligned} &\min_{m_{Pi}\in[m_{Pi}^{min}, m_{Pi}^{max}]} (OF_1, OF_2) \\ &i \in [1, 2\cdots, n_G^{ac}, \cdots, n_G^{ac} + n_G^{ac}] \end{aligned} \tag{27}$$

where OF_1 and OF_2 denote the expected operating cost and the expected emission respectively. They are calculated as given below [23, 41]:

$$\begin{aligned} OF_1 &= E(\sum_{i=1}^{n_G^{ac}+n_G^{dc}} (K_{fueli}f_{fueli} + K_{mi}PG_i)) \\ f_{fueli} &= \frac{PG_i}{\eta_{iP}} \quad \forall i = 1, 2, \cdots, (n_G^{ac} + n_G^{dc}) \\ OF_2 &= E(\sum_{i=1}^{n_G^{ac}+n_G^{dc}} K_{ei}PG_i) \end{aligned} \tag{28}$$

where $E()$ denotes the expectation of a random quantity; K_{fueli}, K_{mi}, η_{iP}, K_{ei}, f_{fueli} are respectively fuel price, maintenance cost, power efficiency, carbon foot print, and fuel consumption of the i^{th}

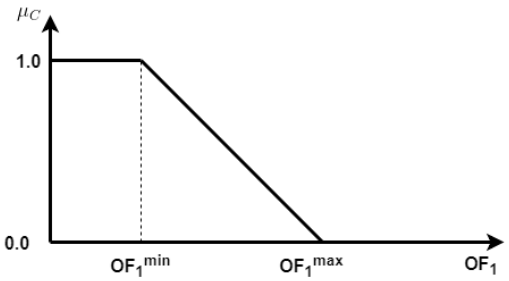

Fig. 2: Membership function for operating cost minimization

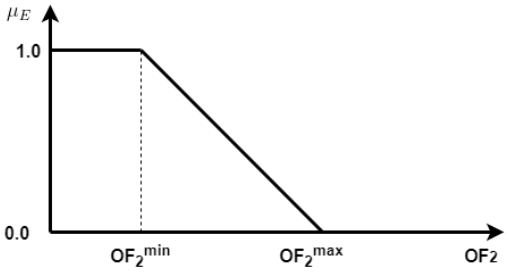

Fig. 3: Membership function for emission minimization

dispatchable unit; n_G^{ac} and n_G^{dc} are numbers of dispatchable units in ACMG and DCMG respectively. The static active power droop constants (m_{Pi}) of the dispatchable units in the AC and the DC subgrids are taken as the design/control variables.

4.2 System constraints

System constraints are given below:

4.2.1 Power balance at each bus: For the ACMG and the DCMG, power (active and reactive for ACMG, active for DCMG) balance at each system bus has to be satisfied. The set of non-linear equations representing the power flow are represented as follows:

$$\begin{aligned} &F_l(g_l, \tau_l) = 0 \quad g_l \in \{c, m\} \\ &\tau_l = \{\tau_l^{ac}, \tau_l^{dc}\} = \{\tau_{il}^{ac}, \tau_{il}^{dc}\} \quad i \in [\Omega_{droop}^{ac}, \Omega_{droop}^{dc}] \\ &\tau_{il}^{ac} = [\omega_{0i}, mp_i, |V_{0i}|, nq_i] \quad i \in \Omega_{droop}^{ac} \\ &\tau_{il}^{dc} = [V_{0i}, mp_i] \quad i \in \Omega_{droop}^{dc} \end{aligned} \tag{29}$$

where $F_l()$ represents set of non-linear power flow equations for loading level l, g_l represents set of power flow state variables, $\tau_l^{ac/dc}$ is the set of droop parameters for AC/DC subsystems, Ω_{droop}^{ac} and Ω_{droop}^{dc} represent the set of all droop buses in ACMG and DCMG respectively, $\{c, m\}$ is allowable range of system state variables.

4.2.2 DG unit rating: Ratings of DG units cannot be exceeded:

$$\begin{aligned} &0 \le PG_i \le PG_i^{max} \quad \forall i \in [\Omega_{DG}^{ac}, \Omega_{DG}^{dc}] \\ &0 \le QG_i \le QG_i^{max} \quad \forall i \in [\Omega_{DG}^{ac}] \end{aligned} \tag{30}$$

4.2.3 Line current limits: Line ratings cannot be exceeded:

$$|I_b| \le I_b^{rated} \quad b \in Nl \tag{31}$$

where $|I_b|$ and I_b^{rated} are respectively the actual current magnitude and the rated current of the b^{th} line, Nl is the set of all lines.

4.2.4 Bus voltage magnitude limits: The bus voltage magnitudes must lie between $0.90p.u.$ and $1.10p.u.$. this is mathematically stated as:

$$0.90p.u. \le |V_i| \le 1.10p.u. \quad \forall i \in [\Omega_{ac}, \Omega_{dc}] \tag{32}$$

4.2.5 Unit ramp up and ramp down limits: Ramp up and ramp down limits of the units are formulated as below:

$$\begin{aligned} &PG_i^t - PG_i^{t-1} \le UR_i \quad \forall i \in [\Omega_{DG}^{ac}, \Omega_{DG}^{dc}] \\ &PG_i^{t-1} - PG_i^t \le DR_i \quad \forall i \in [\Omega_{DG}^{ac}, \Omega_{DG}^{dc}] \end{aligned} \tag{33}$$

where t indicates a time index, UR_i and DR_i are respectively the ramp up and ramp down limits of dispatchable unit i.

5 Solution strategy for optimization problem

Two different optimal solutions exist for the two different objectives (operating cost minimization, and emission minimization), i.e they have conflicting requirements. Usually, when the fuel cost is reduced, the emission becomes high. Also, when the emission is reduced, the fuel cost becomes high. Therefore, when both cost and emission are to be reduced simultaneously, a proper trade-off between cost minimization and emission minimization must be achieved. Zimmermann [28] has shown that a proper trade-off between the conflicting objectives of a multi-objective optimization problem can be attained by representing the objectives in the fuzzy domain.

5.1 Fuzzy membership functions

For solving a multi-objective optimization problem in the fuzzy domain, a membership function is assigned to each objective. Among many possible types of membership functions, it has been noted that a linearly varying membership function is most suitable for solving a multi-objective optimization problem, and therefore, has been used widely [23, 41, 55, 56, 61, 62]. Hence, we have assigned linearly varying membership functions for the cost and emission objectives in this paper. Membership functions can take any value between zero (0) and unity (1). The membership function value is a measure of the extent of achievement of the associated objective. In other words, higher the membership value, better is the extent of achievement of the associated objective. A membership value of unity (the maximum possible value) denotes complete fulfilment of the desired objective. On the other hand, a membership value of zero (the minimum possible value) implies that the corresponding goal has not been achieved at all. A membership value between zero and unity indicates partial realization of the corresponding objective.

5.1.1 Membership function for operating cost minimization: Following membership function is assigned [23, 41, 55, 56]:

$$\begin{aligned} \mu_C &= \frac{OF_1^{max} - OF_1}{OF_1^{max} - OF_1^{min}} \quad OF_1^{min} \le OF_1 \le OF_1^{max} \\ &= 1 \quad OF_1 < OF_1^{min} \\ &= 0 \quad OF_1 > OF_1^{max} \end{aligned} \tag{34}$$

The membership function for cost minimization is shown in Fig.2. If OF_1 is lesser than or equal to OF_1^{min}, then the objective is fully satisfied, and a value of unity is assigned. On the other hand, if OF_1 is greater than or equal to OF_1^{max}, the objective is not fulfilled, and a value of zero is assigned. The membership value varies linearly between zero and unity when OF_1 lies in between OF_1^{max} and OF_1^{min}. A membership value between zero and unity represents partial fulfillment of the economic objective.

5.1.2 Membership function for emission minimization: Membership function for emission minimization is defined as follows [23, 41, 55, 56]:

$$\mu_E = \frac{OF_2^{max} - OF_2}{OF_2^{max} - OF_2^{min}} \quad OF_2^{min} \leq OF_2 \leq OF_2^{max}$$
$$= 1 \quad OF_2 < OF_2^{min}$$
$$= 0 \quad OF_2 > OF_2^{max} \tag{35}$$

The membership function for emission minimization is shown in Fig.3. If OF_2 is lesser than or equal to OF_2^{min}, then the objective is fully satisfied, and a value of unity is assigned. On the other hand, if OF_2 is greater than or equal to OF_2^{max}, the objective is not fulfilled, and a value of zero is assigned. The membership value varies linearly between zero and unity when OF_2 lies in between OF_2^{max} and OF_2^{min}. A membership value between zero and unity represents partial fulfillment of the environmental objective.

Optimal solutions of individual objectives are employed for fixing lower and upper limiting values in (34) and (35). First, optimization problem is solved with cost minimization as the only objective. Obtained values of OF_1 and OF_2 act as lower limiting value in (34) and upper limiting value in (35) respectively. Similarly, optimization problem is solved with emission minimization as the sole objective. Obtained values of OF_1 and OF_2 act as upper limiting value in (34) and lower limiting value in (35) respectively.

5.2 *Multi-objective optimization in the fuzzy domain*

The fuzzy max-min principle [23, 28, 41, 55] is employed for determining the optimal solution of the bi-objective optimization problem. The fuzzy max-min composition is advantageous since good satisfaction of one objective does not overshadow the poor fulfillment of another objective. According to the fuzzy max-min principle, the aggregated objective or the trade-off compromise value is given by the minimum of all the membership values. Since this problem involves two objectives (cost and emission reduction), the trade-off compromise value is provided by the minimum of the membership values corresponding to the economic and emission objectives. At every generation, following steps are followed:

1. For each individual of the population, membership values of the two objectives(μ_C and μ_E) are computed.
2. Least of the two membership values represents the membership value of the aggregated objective:

$$D_{i,iter} = min\{\mu_{C_{i,iter}}, \mu_{E_{i,iter}}\} \tag{36}$$

3. Individual with highest aggregated membership value among the current population is the best candidate solution:

$$S_{iter} = max\{D_{i,iter}\} \quad i \in NP \tag{37}$$

NP is the set of all individuals in the current population.

Particle swarm optimization (PSO) has multiple advantages over other heuristic techniques (e.g., PSO does not require overlapping and mutation computations, good research speed, better optimizing capability, fewer tunable parameters, fast convergence, less computational burden, etc.) [29–33]. Therefore, we have employed PSO as the optimization tool for maximizing S_{iter}.PSO has been discussed extensively in literature [29–32], and hence, it is not elaborated here. However, the PSO update equations are given as below [23, 29–33]:

$$\vec{Vel}_{it} = wt_{pso}\vec{Vel}_{it} + \vec{U}(0,\phi_1) \otimes (\vec{P}_{it} - \vec{X}_{it}) + \vec{U}(0,\phi_2) \otimes (\vec{PG} - \vec{X}_{it}) \tag{38}$$

and

$$\vec{X}_{it} = \vec{X}_{it} + \vec{Vel}_{it} \tag{39}$$

Here, $\vec{U}(0,\phi_j)$ is a vector of random numbers uniformly distributed in $[0,\phi_j]$, and $\otimes$ denotes component wise multiplication. Both the cognitive and social factors (ϕ_1 and ϕ_2) are taken as 2. Both the local and global best lie within the minimum and maximum permissible values of the control variables. In this paper, we have considered the static active power droop coefficients (m_{Pi}) of the dispatchable DG units as the control variables. The maximum value of the static active power constant is determined by the allowable frequency drop and the DG unit ratings. The minimum values of the droop coefficients are taken as 1% of the respective maximum values. Therefore, the local and global best lie within 1% and 100% of the maximum permissible active power droop values.

The optimization program is run in the EMS at regular intervals of time (typically 15 minutes or hourly intervals). In the t^{th} time interval, the forecasted values of loads and renewable generations (with associated uncertainties), network and DG unit characteristics for the next time interval (i.e.$(t+1)^{th}$) are relayed to the EMS through low-bandwidth communication channels. The optimization is carried out in the EMS and the optimal settings are communicated back to the local controllers for implementation. In other words, at the t^{th} time interval, the optimization is carried out for the next i.e. $(t+1)^{th}$ time interval. Since, the optimization is carried out in every 15 minutes/1 hour, the optimization program has to converge within 15 minutes/1hour (depending on whether quarter of an hour ahead or hour ahead optimization is carried out). Although, PSO being a population based technique, is somewhat time consuming, the code converges well within 15 minutes. PSO and other population based evolutionary techniques have been widely used for economic dispatch/optimal scheduling problems in microgrids and traditional power systems [23, 24, 38, 41, 55, 56, 63, 64]. The speed of computation can further be improved by using vectorized PSO, parallel computing techniques [65], and supercomputers.

Hardware implementation of the PSO algorithm can be done using VHSIC Hardware Description Language (VHDL). The components are summarized below [57]:

1. Fitness evaluation block: Fitness is calculated for all the particles and the local and the global bests are updated in parallel.
2. Position block: Positions of the particles are calculated and updated as per (39). The updated positions are stored in the memory.
3. Velocity block: Velocities of the particles are calculated and updated as per (38). The updates are stored in the memory. In this block, random number generators generate random numbers using linear feedback shift register (LFSR) with XOR feedback.
4. Control unit: For synchronization and control of operations between the above three components.
5. Memory: For storage of calculations and updates.

Further details on hardware implementation of PSO are available in [57–60]. Figure 4 shows the block diagram of the hardware architecture for implementation of PSO [57].

6 Simulation results

6.1 *Test system*

A 6 bus test ADHMG system [9] is used for simulation study. The system comprises a 3 bus AC sub-system and a 3 bus DC subsystem interlinked by a bi-directional interlinking converter. Fig.5 shows the test system. Line data is available in [9]. ACMG comprises two droop-controlled units (a natural gas turbine (NGT) and a biomass unit) and a wind turbine (WT) generator. The wind generator follows MPPT algorithm, and operates as a leading power factor (0.80 power factor leading) DG unit, i.e. it delivers active power but absorbs reactive power from the network. DCMG comprises two droop-controlled units (natural gas fuel cell (NGFC) and biomass) and a solar photovoltaic (SPV) DG unit. The SPV follows MPPT and operates at unity power factor. Nominal system voltages are 208 V and 600 V respectively for AC and DC sub-systems. Interlinking converter has a rating of 6.25 kVA and is allowed to exchange a maximum of 5 kW power between AC and DC sub-systems. The bi-directional interlinking converter is present connected between

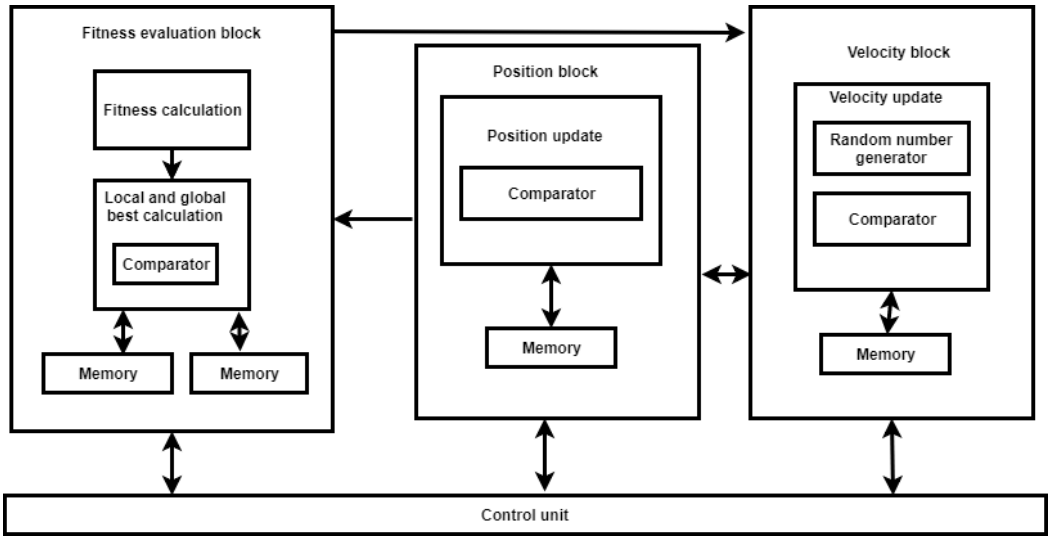

Fig. 4: Block diagram of PSO algorithm architecture [57]

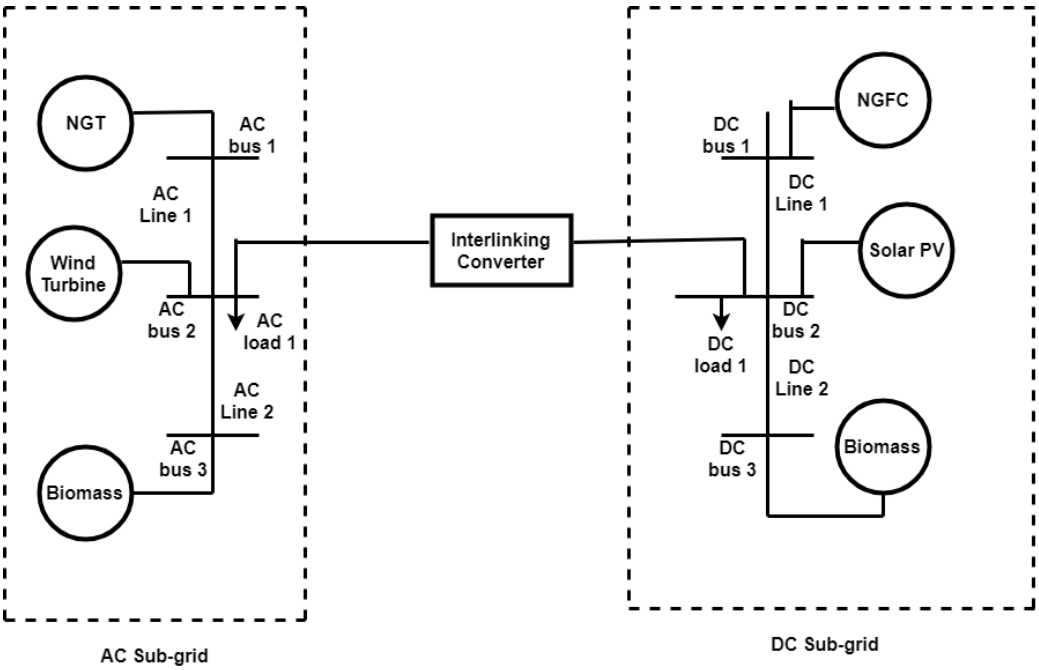

Fig. 5: Test system

DC bus 2 and AC bus 2. The nominal system load in the ACMG is 25 kW and 18.75 kVar (at AC bus number 2). The nominal system load in the DCMG is 15 kW (at DC bus number 2). DG unit details are given in Table 1. The dispatchable unit parameters are based on date available in [23, 41, 55, 56]. For simulation, we have considered the following parameters: $k = 5m/s$, $c = 7m/s$, $v_{ci} = 3m/s$, $v_r = 12m/s$, $v_{furl} = 25m/s$, $\mu_s = 0.7305kW/m^2$, and $\sigma_s = 0.1510kW/m^2$, $\mu_L = 1.0p.u$ and $\mu_L = 0.05p.u$.

6.2 *Simulation results*

Active power droop constants (m_{Pi}) of dispatchable DG units in ACMG and DCMG are taken as optimization parameters. Following simulation studies were carried out:

Table 1 DG unit parameters

DG Type	NGT	Wind	Biomass	NGFC	PV
Bus	AC1	AC2	AC3/DC3	DC1	DC2
η_{iP} (p.u)	0.37	N/A	0.285	0.339	N/A
K_{ei} (kgCO2/MWh)	201.6	N/A	3	366.1	N/A
K_{fueli} ($/MWh)	20.5	N/A	63	20.5	N/A
K_{mi} ($/MWh)	3	N/A	12	34	N/A
PG_i^{max}(kW)	18	14	18/12.50	12.50	4.6
QG_i^{max}(kVAr)	13.50	10.5	13.50/N/A	N/A	N/A
m_{Pi}(pu)	0.01	N/A	0.01/0.072	0.072	N/A
n_{Qi}(pu)	0.0667	N/A	0.0667/N/A	N/A	N/A

[a] Maximum values/base case values

Table 2 Expected values of cost and emission

Cost and emission in base case and different scenarios				
Scenarios	Base case	S1	S2	S3
Operating cost($\$/hr$)	4.9027	3.1439	6.8496	4.6938
Emission ($kgco_2/hr$)	4.0744	6.8609	1.0962	3.5078

Table 3 Active power outputs of dispatchable units and IC

Units	Expected power outputs (kW)		
Scenarios	S1	S2	S3
NGT(ACMG)	10.42	1.47	8.46
Biomass(ACMG)	1.64	10.37	2.90
NGFC(DCMG)	5.16	0.81	0.83
Biomass(DCMG)	1.51	6.09	6.42
Interlinking converter	-0.24	-0.01	0.35

Table 4 Optimized static active power droop constants

Units	Static active power droop constants (per unit)		
Scenarios	S1	S2	S3
NGT(ACMG)	0.000100	0.010000	0.003400
Biomass(ACMG)	0.010000	0.000100	0.010000
NGFC(DCMG)	0.000720	0.072000	0.072000
Biomass(DCMG)	0.072000	0.000720	0.000720

Table 5 Expected magnitude of line currents

Units	Expected Line current magnitudes (A)		
Scenarios	S1	S2	S3
AC Line 1	59.34	9.90	43.03
AC Line 2	11.71	59.35	25.21
DC Line 1	14.75	2.27	2.39
DC Line 2	4.30	17.34	18.27

1.Base case: Here the static active power droop constants are set as per the capacity ratings of the dispatchable DG units, i.e., droop constants are in the inverse ratio of the ratings of the units. In other words, the droop settings are set so that the dispatchable units share active power in the proportion of their ratings. So, a unit with a higher rating has a lower value of static active power droop constant.
2.Scenario 1 (S1): Static active power droop values are optimized for minimizing operating cost only.
3.Scenario 2 (S2): Static active power droop values are optimized for minimizing emission only.
4.Scenario 3 (S3): Static active power droop values are optimized for simultaneous minimization of operating cost end emission.

For all simulation scenarios, feasible values of static active power droop constants are are assumed to lie between 1% and 100% of the maximum values. Expected operating costs and emissions in different scenarios are given in Table 2. Table 3 gives estimated values of active power outputs of all dispatchable units in different scenarios.

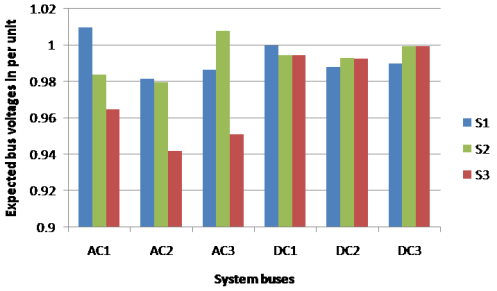

Fig. 6: Expected bus voltages in different scenarios

Table 4 gives the optimized values of static active power droop constants of the dispatchable units in different scenarios. Following are observed from Table 2:

1.In S1, the objective is to minimize operating cost. Therefore, from Table 2, it is observed that operating cost is minimum for this scenario. In comparison to the base case scenario, the operating cost reduces by 35.87%. However, for S1, emission is highest. Emission increases by 68.39% of the base case value. This is because, cost and emission minimization are conflicting objectives.
2.Objective in S2 is to minimize emission. Therefore, emission is least among the three scenarios. Emission in this case is only 15.98% of the emission value in S1. In comparison to the base case, emission is reduced by 73.10%. But reduction in emission is accompanied by an increase in operating cost. Operating cost for S2 is the highest among all the simulated scenarios. Operating cost is 217.87% of that in S1. In comparison to the base case, operating cost increases by 39.71%.
3.Objective in S3 is to simultaneously minimize operating cost and emission. So this is a compromise solution. Operating cost in this case is 149.31% of that in S1 and 68.53% of that in S2. In comparison to the base case, the operating cost reduces by 4.26%, while the emission reduces by 13.91%. In other words, operating cost in S3 is in-between those in S1 and S2. Similarly, emission in S3 is 51.12% of that in S1 and 319.97% of that in S2. Therefore, this scenario yields a compromise or trade-off between cost and emission minimization.

The expected bus voltages in different scenarios are shown in Fig.6. It is observed that in all the scenarios, all the bus voltages are within acceptable limits. Thus, the system inequality constraints are satisfied.

From Table 3 and Table 4, following are observed:

1.NGT and NGFC units have smaller values of static active power droop constants in scenario S1 in comparison to scenario S2 (refer to Table 4). In other words, NGT and NGFC units generate more power in scenario S1 (objective in S1 is cost minimization) than in scenario S2 (objective in S2 is emission minimization). On the other hand, biomass units generate more power (and hence smaller values of static active power droop constant) in scenario S2 than in scenario S1. This is attributable to the fact the NGT and NGFC units have better power efficiencies in comparison to biomass unit (refer to Table 1). Moreover, fuel cost (natural gas) for NGFC and NGT is lower than the fuel cost of biomass unit. Therefore, whenever the objective is to minimize operating cost (scenario S1), NGT and NGFC tend to share the bulk of the active load. Biomass unit being a comparatively expensive power source generates lesser power. On the other hand, carbon footprint of biomass unit is much lower than those of NGT and NGFC (refer to Table 1). Therefore, for satisfaction of environmental objective (scenario S2 where the objective is to minimize emission), biomass unit generates bulk of the active power, and NGT and NGFC units generate smaller amounts of active power.

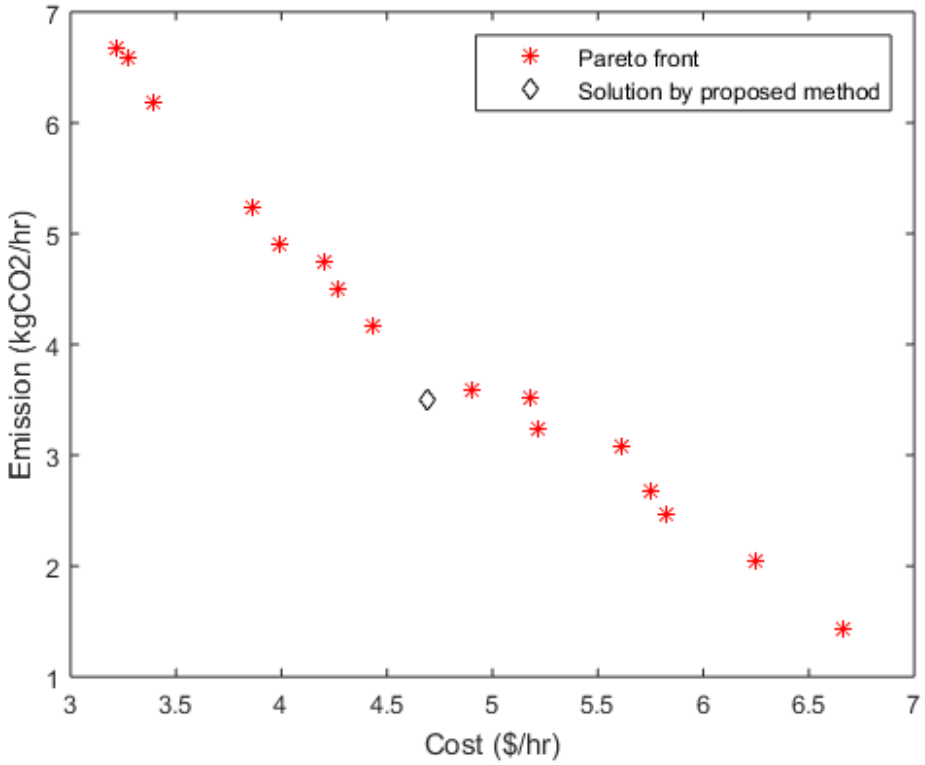

Fig. 7: Pareto front obtained by controlled elitist multi-objective genetic algorithm

2.Total power generated in the DCMG in scenario S3 is higher than that in scenario S1 and S2. Also, total power generated in the ACMG in scenario S3 is lesser than that in scenarios S1 and S2. Load remains same for all the three scenarios. Therefore, in scenario S1 and S2, active power is transferred from AC to DC sub-grid via the interlinking converter. On the other hand, in scenario S3, active power is transferred from DC to AC side.

Table 5 shows the expected current magnitude through different lines in different scenarios. Following are observed from Table 5:

1.In scenario S1, AC line 1 carries more current in comparison to AC line 2; DC Line 1 carries larger current than DC Line 2. That is because, in Scenario S1, NGT (connected to AC bus 1) and NGFC (connected to DC bus 1) generate more power in comparison to Biomass units (connected to AC bus 3 and DC bus 3). Therefore, to feed the loads (connected to AC bus 2 and DC bus 2), AC line 1 (connected between AC bus 1 and AC bus 2) and DC line 1 (connected between DC bus 1 and DC bus 2) carry more currents in comparison to AC line 2 (connected between AC bus 2 and AC bus 3) and DC line 2 (connected between DC bus 2 and DC bus 3) respectively.
2.In scenario S2, AC line 2 carries more current in comparison to AC line 1; DC Line 2 carries larger current than DC Line 1. That is because, in Scenario S2, Biomass units (connected to AC bus 3 and DC bus 3) generate more power in comparison to NGT (connected to AC bus 1) and NGFC (connected to DC bus 1) units. Therefore, to feed the loads (connected to AC bus 2 and DC bus 2), AC line 2 (connected between AC bus 2 and AC bus 3) and DC line 2 (connected between DC bus 2 and DC bus 3) carry more currents in comparison to AC line 1 (connected between AC bus 1 and AC bus 2) and DC line 1 (connected between DC bus 1 and DC bus 2) respectively.
3.In Scenario S3, current magnitudes through the lines lie in between the values obtained in scenarios S1 and S2. Aforementioned is attributable to the fact that scenario S3 is a compromise or trade-off between scenarios S1 and S2.

Table 6 Results for cost prioritized droop scheme

Systems	ACMG		DCMG	
Units	NGT	Biomass	NGFC	Biomass
m_{Pi} (per unit)	0.005	0.01	0.0288	0.072
Expected Generation (kW)	7.86	3.93	4.15	2.60
Expected Cost ($\$/hr$)			4.0803	
Expected Emission ($kgco_2/hr$)			5.3699	

Table 7 Results for emission prioritized droop scheme

Systems	ACMG		DCMG	
Units	NGT	Biomass	NGFC	Biomass
m_{Pi} (per unit)	0.01	0.005	0.072	0.00059
Expected Generation (kW)	3.70	7.38	0.86	6.60
Expected Cost ($\$/hr$)			6.1102	
Expected Emission ($kgco_2/hr$)			1.8891	

6.3 Validation by comparison with other methods

6.3.1 Validation of results for Scenario S1: The objective in this case is to minimize the operating cost. For validating the results obtained for this scenario, we have made a comparison with cost -prioritized droop settings [66]. The cost-prioritized droop values, expected active power generations from the dispatchable units, the expected cost, and the expected emission are given in Table 6. It is observed that, with cost-prioritized droop scheme, the operating cost reduces by about 16.77% in comparison to the base case. On the other hand, by the proposed method a cost saving of 35.87% (scenarios S1) can be achieved. Therefore, the proposed scheme is more effective in comparison to the cost-prioritized droop scheme.

6.3.2 Validation of results for Scenario S2: The objective in this case is to minimize the emission. To the best of the author's knowledge, there is no published work that deals with emission minimization in an ADHMG. Therefore, a direct comparison is not possible. However, for validation, we have developed a method similar to the cost-prioritized droop settings [66]. We follow the same steps as in cost-prioritized droop scheme, but replace the cost function by the emission function (since emission reduction, and not cost reduction is the objective). The droop settings obtained by this method is named as the emission-prioritized droop scheme. The results are given in Table 7. It is noted that the emission-prioritized droop scheme results in a reduction of emission by 53.63% from the base case. On the other hand, a reduction in emission by 73.10% is possible with the proposed method. Therefore, the proposed method yields better results.

6.3.3 Validation of results for Scenario S3: The objective in this case is to minimize the operating cost and the emission simultaneously. To the best of the author's knowledge, no similar work has been reported so far. Therefore, a direct comparison is not possible. However, we can solve the bi-objective optimization problem by any well established multi-objective optimization solver tool. If the solution (by the proposed method) lies on the pareto front (yielded by the well established multi-objective optimizer), then it can be concluded that the obtained solution is optimal. Therefore, the proposed method can be indirectly verified. Controlled elitist multi-objective genetic algorithm [67] is one such widely accepted and used multi-objective optimization solving algorithm. Therefore, for verifying whether the solution yielded by the proposed method lies on the pareto front, we have solved the bi-objective optimization problem using controlled elitist multi-objective genetic algorithm [67]. The pareto front (from controlled elitist multi-objective genetic algorithm) as well as the solution yielded by the proposed algorithm are shown in Fig.7. From Fig.7, we note that the trade-off optimal solution yielded by the suggested method lies on the pareto front. Thus a comparison with well-established controlled elitist multi-objective GA vindicates the method suggested in this paper. In comparison to controlled elitist multi-objective GA, it is easier to write programs for the suggested method. Therefore, the advantage of the proposed method lies in its simplicity.

7 Conclusion

ADHMG is gradually emerging as a popular choice for serving an area with DC and AC loads and sources. For financial and environmental benefits, it is necessary to operate an ADHMG with reduced cost and emission. This paper introduces a method of determining optimal values of static active droop power constants in an ADHMG to simultaneously reduce cost and emission under load and generation uncertainties. To obtain an accurate steady state picture of the system, primary droop control of dispatchable units in the AC and DC sub-systems, and the function of the interlinking converter have been incorporated in the optimal dispatch problem by using a power flow algorithm tailor-made for ADHMG. Further, load and generation uncertainties have been incorporated in the optimal scheduling problem by using Hong's $2m$ PEM. Load has been modeled using normal distribution, wind speed has been modeled using Weibull distribution and solar irradiance has been represented by beta distribution. Two objectives (cost minimization and emission minimization) have been translated to fuzzy domain by assigning membership function to each objective. The fuzzy membership value of the aggregated objective is the least of the two membership values. Membership value of the aggregated objective has been maximized using PSO. Simulation studies have been carried out using a 6 bus test ADHMG system. Simulation results show that a maximum cost saving of about 35.87% and a maximum reduction of emission by approximately 73.10% can be achieved by optimally setting the static active power droop constants. The reduction in cost and emission are found to be more with the proposed method in comparison to cost-prioritized droop scheme and emission-prioritized droop scheme respectively. For simultaneous reduction of cost and emission, a cost saving of 4.26% and a reduction in emission by about 13.91% can be achieved in comparison to capacity based droop settings for the given system. Moreover, a comparison with the controlled elitist multi-objective GA demonstrates that the optimal solution as obtained by the proposed method lies on the pareto front. Simplicity in coding and implementation of the proposed method is its main advantage. In future, the present work may be expanded to investigate the possible benefits of participation of storage devices in scheduling under load and generation uncertainties for economic-emission dispatch in an ADHMG.

8 References

1 Liu, X., Wang, P., Loh, P.C. : 'A hybrid AC/DC microgrid and its coordination control', IEEE Transactions on Smart Grid, 2011, 2, (2), pp.278–286
2 Loh, P. C., Li, D., Chai, Y. K., et al.: 'Autonomous operation of hybrid microgrid with AC and DC subgrids', IEEE transactions on power electronics, 2013, 28,(5), pp. 2214–2223
3 Eghtedarpour, N., Farjah, E. : 'Power control and management in a hybrid AC/DC microgrid', IEEE transactions on smart grid, 2014, 5, (3), pp. 1494–1505
4 Guerrero, J. M., Vasquez, J. C., Matas, J., et al.: 'Hierarchical control of droop-controlled AC and DC microgridsÜA general approach toward standardization', IEEE Transactions on industrial electronics, 2011, 58, (1), pp. 158–172
5 Lopes, J. P., Moreira, C. L., mMadureira, A. G.: 'Defining control strategies for microgrids islanded operation', IEEE Transactions on power systems, 2006, 21, (2), pp. 916–924
6 Guerrero, J. M., Chandorkar, M., Lee, T. L., et al.: 'Advanced control architectures for intelligent microgrids-Part I: Decentralized and hierarchical control', IEEE Transactions on Industrial Electronics, 2013, 60, (4), pp. 1254–1262
7 Nejabatkhah, F., Li, Y. W.: 'Overview of power management strategies of hybrid AC/DC microgrid', IEEE Transactions on Power Electronics, 2015, 30, (12), pp. 7072–7089
8 Li, C., Chaudhary, S. K., Vasquez, J. C., et al.: 'Power flow analysis for droop controlled LV hybrid AC-DC microgrids with virtual impedance'. IEEE PES General Meeting Conference and Exposition, Washington, USA, July 2014, pp. 1–4)
9 Eajal, A. A., Abdelwahed, M. A., El-Saadany, E. F., et al.: 'Power flow analysis of AC/DC hybrid microgrids'. IEEE Electrical Power and Energy Conference (EPEC), Ottawa, Canada, October 2016, pp. 1–6
10 Eajal, A. A., Abdelwahed, M. A., El-Saadany, E. F., et al.: 'A unified approach to the power flow analysis of AC/DC hybrid microgrids',IEEE Transactions on Sustainable Energy, 2016, 7, (3), pp.1145–1158
11 Hamad, A. A., Azzouz, M. A., El Saadany, E. F.: 'A sequential power flow algorithm for islanded hybrid AC/DC microgrids', IEEE Transactions on Power Systems, 2016, 31, (5), pp.3961–3970
12 Nassar, M. E., Hamad, A. A., Salama, M. M. A., et al.: 'A Novel Load Flow Algorithm for Islanded AC/DC Hybrid Microgrids', IEEE Transactions on Smart Grid, 2017, DOI:10.1109/TSG.2017.2772263
13 Ahmed, H. M., Eltantawy, A. B., Salama, M. M. A.: 'A Generalized Approach to the Load Flow Analysis of AC/DC Hybrid Distribution Systems', IEEE Transactions on Power Systems, 2018, 33, (2), pp.2117–2127
14 Baboli, P. T., Shahparasti, M., Moghaddam, M. P., et al.: 'Energy management and operation modelling of hybrid AC-DC microgrid', IET Generation, Transmission and Distribution, 2014, 8, (10), pp.1700–1711
15 Hosseinzadeh, M., Salmasi, F. R.: 'Power management of an isolated hybrid AC/DC micro-grid with fuzzy control of battery banks', IET Renewable Power Generation, 2015, 9, (5), pp.484–493
16 Hosseinzadeh, M., Salmasi, F. R.: 'Robust optimal power management system for a hybrid AC/DC micro-grid', IEEE Transactions on Sustainable Energy, 2015, 6, (3), pp.675–687
17 Li, P., Hua, H., Di, K., et al.: 'Optimal operation of AC/DC hybrid microgrid under spot price mechanism'. IEEE Power and Energy Society General Meeting (PESGM), Boston, USA, July 2016, pp. 1–5
18 Peng, L. I., Pengfei, H. A. N., Shuai, H. E., et al.: 'Double-uncertainty optimal operation of hybrid AC/DC microgrids with high proportion of intermittent energy sources', Journal of Modern Power Systems and Clean Energy, 2017, 5, (6), pp.838–849
19 Qi, C., Wang, K., Fu, Y., et al.: 'A Decentralized Optimal Operation of AC/DC Hybrid Distribution Grids', IEEE Transactions on Smart Grid, 2017, DOI:10.1109/TSG.2017.2703582

20 Hussain, A., Bui, V. H., Kim, H. M.: 'Robust Optimal Operation of AC/DC Hybrid Microgrids Under Market Price Uncertainties', IEEE Access, 2018, 6, pp.2654–2667
21 Energy, I.E.A.: 'Climate change: world energy outlook special briefing for COP21', (International Energy Agency, Paris, 2015)
22 International Energy Agency (IEA): 'CO2 emissions from fuel combustion' (International Energy Agency, Paris, 2017)
23 Maulik, A., Das, D.: 'Optimal Operation of a Droop-Controlled DC Microgrid with Generation and Load Uncertainties', IET Generation, Transmission and Distribution, 2018, 12, (12), pp. 2905–2917
24 Niknam, T., Golestaneh, F., Malekpour, A.: 'Probabilistic energy and operation management of a microgrid containing wind/photovoltaic/fuel cell generation and energy storage devices based on point estimate method and self-adaptive gravitational search algorithm', Energy, 2012, 43, (1), pp. 427–437
25 Soroudi, A., Amraee, T.: 'Decision making under uncertainty in energy systems: State of the art,' Renewable and Sustainable Energy Reviews, 2013, 28, pp. 376–384
26 Aien, M., Hajebrahimi, A., Fotuhi-Firuzabad, M.: 'A comprehensive review on uncertainty modeling techniques in power system studies', Renewable and Sustainable Energy Reviews, 2016, 57, pp. 1077–1089
27 Bahrami, S. and Amini, M.H.: 'A decentralized trading algorithm for an electricity market with generation uncertainty', Applied Energy, 2018, 218, pp.520–532
28 Zimmermann, H. J.: 'Fuzzy programming and linear programming with several objective functions', Fuzzy sets and systems, 1978, 1, (1), pp.45–55
29 Kennedy, J., Eberhart, R.C.: 'Particle swarm optimisation'. Proc. IEEE Int. Conf. Neural Networks, Piscataway, NJ, 1995, pp. 1942Ű-1948
30 Bai, Q.: 'Analysis of particle swarm optimisation algorithm', Comput. Inf. Sci., 2010, 3, (1), pp. 180–184
31 Poli, R., Kennedy, J., Blackwell, T.: 'Particle swarm optimisation', Swarm Intell., 2007, 1, (1), pp. 33Ű-57
32 Clerc, M.: 'Particle swarm optimisation', vol. 93, (John Wiley and Sons, Hoboken, NJ, USA, 2010)
33 Maulik, A., Das, D.: 'Optimal operation of microgrid using four different optimization techniques', Sustainable Energy Technologies and Assessments, 2017, 21, pp.100–120
34 Rosenblueth, E.: 'Point estimates for probability moments', Proc. Natl. Acad. Sci., 1975, 72, (10), pp. 3812Ű-3814
35 Harr, M.E.: 'Probabilistic estimates for multivariate analyses', Appl. Math. Model., 1989, 13, (5), pp. 313Ű-318
36 Hong, H.P.: 'An efficient point estimate method for probabilistic analysis', Reliab. Eng. Syst. Saf., 1998, 59, (3), pp. 261Ű-267
37 Evangelopoulos, V.A., Georgilakis, P.S.: 'Optimal distributed generation placement under uncertainties based on point estimate method embedded genetic algorithm', IET Gener. Trans. Distrib., 2013, 8, (3), pp. 389Ű-400
38 Mohammadi, S., Mozafari, B., Solimani, S.: 'Optimal operation management of microgrids using the point estimate method and firefly algorithm while considering uncertainty', Turk. J. Electr. Eng. Comput. Sci., 2014, 22, (3), pp. 735-Ű753
39 Su, C.L.: 'Probabilistic load-flow computation using point estimate method', IEEE Trans. Power Syst., 2005, 20, (4), pp. 1843Ű-1851
40 Su, C.L., Lu, C.N.: 'Two-point estimate method for quantifying transfer capability uncertainty', IEEE Trans. Power Syst., 2005, 20, (2), pp. 573Ű-579
41 Maulik, A., Das, D.: 'Optimal operation of droop-controlled islanded microgrids', IEEE Transactions on Sustainable Energy, 2018, 9, (3), pp. 1337–1348
42 Salameh, Z.M., Borowy, B.S. and Amin, A.R.: 'Photovoltaic module-site matching based on the capacity factors', IEEE transactions on Energy conversion, 1995, 10, (2), pp.326–332
43 Atwa, Y.M., El-Saadany, E.F., Salama, M.M.A., et al.: 'Optimal renewable resources mix for distribution system energy loss minimisation', IEEE Trans. Power Syst., 2010, 25, (1), pp. 360-Ű370
44 Teng, J.H., Luan, S.W., Lee, D.J., et al. 'Optimal charging/discharging scheduling of battery storage systems for distribution systems interconnected with sizeable PV generation systems', IEEE Trans. Power Syst, 2013, 28, (2), pp.1425–1433
45 Hung, D.Q., Mithulananthan, N. and Bansal, R.C.: 'Integration of PV and BES units in commercial distribution systems considering energy loss and voltage stability', Applied Energy, 2014, 113, pp.1162–1170
46 Tan, S., Xu, J.X. and Panda, S.K.: 'Optimization of distribution network incorporating distributed generators: An integrated approach', IEEE Transactions on power systems, 2013, 28, (3), pp.2421–2432
47 Hung, D.Q., Mithulananthan, N. and Lee, K.Y., 'Determining PV penetration for distribution systems with time-varying load models', IEEE Transactions on Power Systems, 2014, 29, (6), pp.3048-3057
48 Cheng, Y.S., Chuang, M.T., Liu, Y.H., et al. 'A particle swarm optimization based power dispatch algorithm with roulette wheel re-distribution mechanism for equality constraint', Renewable Energy, 2016, 88, pp.58–72
49 Hetzer, J., David, C.Y. and Bhattarai, K.: 'An economic dispatch model incorporating wind power', IEEE Transactions on energy conversion, 2008, 23, (2), pp.603-611
50 Roy. S: 'Market Constrained Optimal Planning for Wind Energy Conversion Systems Over Multiple Installation Sites', IEEE Transactions on energy conversion, 2002, 17, (1), pp. 124–129
51 Dong, L., Cheng, W., Bao, H., et al.: 'Probabilistic load flow analysis for power system containing wind farms', IEEE Asia-Pacific Power and Energy Engineering Conference (APPEEC), Chengdu, China, 2010, pp. 1–4
52 Mohammadi, S., Soleymani, S. and Mozafari, B.: 'Scenario-based stochastic operation management of microgrid including wind, photovoltaic, micro-turbine, fuel cell and energy storage devices', International Journal of Electrical Power and Energy Systems, 2014, 54, pp.525–535
53 Mohammadi, S., Mozafari, B., Solimani, S., et al.: 'An Adaptive Modified Firefly Optimisation Algorithm based on Hong's Point Estimate Method to optimal operation management in a microgrid with consideration of uncertainties', Energy, 2013, 51, pp.339–348
54 Bo, R., Li, F.: 'Probabilistic LMP forecasting considering load uncertainty', IEEE Transactions on Power Systems, 2009, 24, (3), pp.1279–1289
55 Maulik, A., Das, D.: 'Economic-emission dispatch of a droop-controlled DC microgrid', IEEE Region 10 Conference (TENCON 2017), Penang, Malaysia, Nov.2017, pp. 72–77
56 Gabbar, H.A., Zidan, A.: 'Optimal scheduling of interconnected micro energy grids with multiple fuel options', Sustain. Energy Grids Netw., 2016, 7, pp. 80Ű-89
57 Morsi, N.N., Abdelhalim, M.B. and Shehata, K.A.: 'Efficient hardware implementation of PSO-based object tracking system', International Conference on Electronics, Computer and Computation (ICECCO), Ankara/Turkey, Nov.2013, pp. 155–158
58 Liu, L., Liu, W., Cartes, D.A., et al.: , 2008, June. 'Real time implementation of particle swarm optimiation based model parameter identification and an application example', IEEE Congress on Evolutionary Computation (IEEE World Congress on Computational Intelligence), Hongkong, 2008, pp. 3480–3485
59 Talaska, T., Dlugosz, R. and Pedrycz, W.: 'Hardware implementation of the particle swarm optimization algorithm', 24th International Conference on Mixed Design of Integrated Circuits and Systems, Bydgoszcz, Poland, June 2017 pp. 521–526
60 Lu, Y., Wang, P. and Qin, J.: 2017. 'A hardware architecture of particle swarm optimization', Journal of Computers, 2017, 12, (5), pp.442–450
61 Niknam, T., Kavousifard, A., Aghaei, J.: 'Scenario-based multiobjective distribution feeder reconfiguration considering wind power using adaptive modified particle swarm optimisation', IET Renew. Power Gener., 2012, 6, (4), pp. 236-Ű247
62 Das, D.: 'A fuzzy multiobjective approach for network reconfiguration of distribution systems', IEEE Trans. Power Deliv., 2006, 21, (1), pp. 202Ű-209
63 Li, C., de Bosio, F., Chen, F., et al.: 'Economic dispatch for operating cost minimisation under real-time pricing in droop-controlled DC microgrid',IEEE J. Emerging Sel. Top. Power Electron., 2017, 5, (1), pp. 587Ű595
64 Mahor, A., Prasad, V. and Rangnekar, S.: 'Economic dispatch using particle swarm optimization: A review', Renewable and sustainable energy reviews, 2009, 13, (8), pp.2134–2141
65 McNabb, A.W., Monson, C.K. and Seppi, K.D.: 2007, September. 'Parallel PSO using MapReduce', IEEE Congress on Evolutionary Computation, Spetember 2007, pp. 7–14
66 Nutkani, I.U., Loh, P.C., Wang, P., et al.: 'Cost-prioritized droop schemes for autonomous AC microgrids', IEEE Transactions on Power Electronics, 2015, 30, (2), pp.1109–1119
67 Deb. K., Goel.T.: 'Controlled elitist non-dominated sorting genetic algorithms for better convergence'. Evolutionary multi-criterion optimization, Springer Berlin/Heidelberg, March 2001, pp. 67–81